DRAFT SF 298

1. Report Date (dd-mm-yy)	2. Report Type	3. Dates covered (from... to)
4. Title & subtitle The Use of Superconducting Magnetometry to Detect Corrosion in Aircraft Alloys Tri-Service Committee on Corrosion Proceedings		5a. Contract or Grant # 5b. Program Element #
6. Author(s) Delin Li, Yupei Ma, W. F. Flanagan, B. D. Lichter, J. P. Wikswo, Jr.		5c. Project # 5d. Task # 5e. Work Unit #
7. Performing Organization Name & Address		8. Performing Organization Report #
9. Sponsoring/Monitoring Agency Name & Address Tri-Service Committee on Corrosion USAF WRIGHT-PATTERSON Air Force Base, Ohio 45433		10. Monitor Acronym 11. Monitor Report #
12. Distribution/Availability Statement Approved for Public Release Distribution Unlimited		
13. Supplementary Notes		
14. Abstract 		
15. Subject Terms Tri-Service Conference on Corrosion		

Security Classification of			19. Limitation of Abstract	20. # of Pages	21. Responsible Person (Name and Telephone #)
16. Report	17. Abstract	18. This Page			

TRI-SERVICE CONFERENCE ON CORROSION

21-23 JUNE 1994

SHERATON PLAZA HOTEL
ORLANDO, FLORIDA

PROCEEDINGS

The Use of Superconducting Magnetometry to Detect Corrosion In Aircraft Alloys

Delin Li[a], Yupei Ma[b], W. F. Flanagan[a], B. D. Lichter[a], and J.P. Wikswo,Jr[b*]
a. Department of Mechanical Engineering
b. Department of Physics and Astronomy
Vanderbilt University, Nashville, TN 37235

Abstract

The magnetic field distribution for three different types of in-situ corrosion has been measured using SQUID magnetometry. The variations of the magnetic field density with time differ for the three types of corrosion. The higher the corrosion rate, the more intense is the magnetic field. The SQUID magnetometer is also shown to be sensitive to corrosion activity occurring on the opposite side of a plate specimen.

1. Introduction

Over the last few decades, there have been many attempts to measure the corrosion current distribution during active corrosion, with little success. Since the net anodic current is equal to the net cathodic current in active corrosion, any non-local measuring methods would sense a net current approaching zero. By using a scanning reference electrode (SRE) technique[1-5], there has been some success in measuring the corrosion potential distribution on actively corroding samples. However, such results do not give directly the resulting corrosion current distribution, since many factors are involved in the interpretation of the data, not all of which are known.

It is recognized that magnetic fields are associated with current flow. Thus, the corrosion current should have an associated magnetic signature. The detectability of the magnetic fields depends on the magnitude and the spatial distribution of the corrosion current. The SQUID magnetometer enables sensitive

measurements of extremely small magnetic fields to be made non-invasively, that is, without any electrical or mechanical connections intruding on the sample. It offers the promise of monitoring both the magnitude and the spatial distribution of the corrosion current, which present corrosion methods do not allow. The ability of the SQUID magnetometer to measure magnetic signals due to electrochemical reactions has been proven recently[6-10]. The Vanderbilt Superconducting Quantum Interference Device (SQUID) magnetometer system, which incorporates a MicroSQUID magnetometer[11], a magnetic shield[12], a scanning stage[13], and a computer control and data acquisition system[14], has been developed and used for the detection of flaws in nonferromagnetic conductors[14,15], and for the detection of subsurface flaws[16]. In the present paper, we focus on the application of SQUID magnetometry to the detection and mapping of the magnetic field distribution on active in-situ corroding aluminum alloys used in the manufacture of aircraft. The analysis of these data in terms of the corrosion current distribution will be reported in a later paper.

2. Experimental

Three types of active corrosion were studied: pitting corrosion, pitting/intergranular corrosion, and "uniform" corrosion. Pitting corrosion was modeled using 1.5 mm thick 7075 aluminum alloy in solutions of 3.5% NaCl with differing Cu^{++} concentrations. Pitting/intergranular corrosion was modeled using 1.5 mm thick 2024 aluminum alloy in solutions of 3.5% NaCl with differing Cu^{++} concentrations. "Uniform" corrosion was modeled using 1.5 mm thick 2024 aluminum alloy in a solution of 2 ml 58% HF, 3 ml 71% HNO_3, 5 ml 36.5% HCl, and 590 ml H_2O.

The physical details of the SQUID tests are shown in Figure 1a and 1b, respectively. For tests described by Figure 1a, the sample was placed in the corrosion cell with the solution extending to 2 mm above the sample surface. The corrosion cell was covered by a transparent film which served to protect the SQUID detector from the corrosive environment. The SQUID pick-up coils were located about 3 mm above the plastic film. Thus, the distance between the SQUID pick-up coils and the sample was about 5 mm. For tests described in Figure 1b, a large plate sample was placed on the corrosion cell, which had an 45 mm diameter area exposed to the solution, but on the bottom side of the plate, on the side opposite from the SQUID magnetometer. For this test, the SQUID pick-up coils were located 4 mm above the top sample surface. All aluminum alloy plates used in the tests were 1.5 mm thick. It should also be noted that the SQUID measures only the vertical component of the magnetic field, normal to the corroding surface.

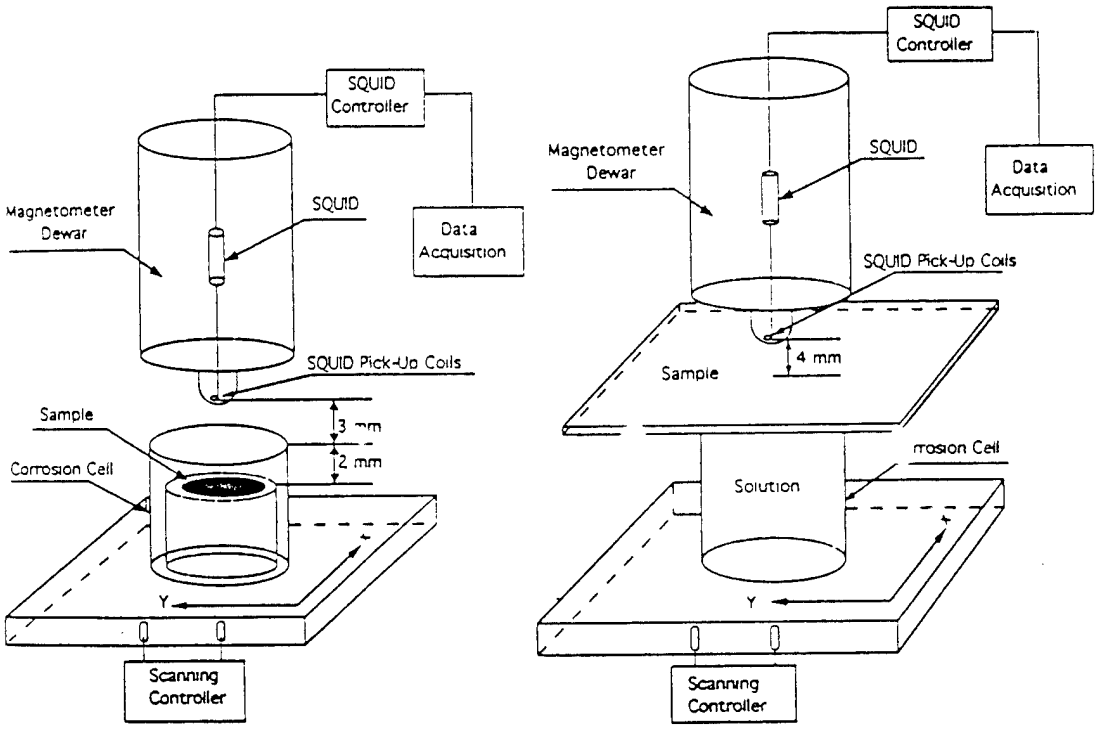

Figure 1. Schematic diagrams of the active in-situ corrosion test systems: a) The sample is placed in a corrosion cell so that the top surface is 2 mm below the solution surface; b) a large plate sample which has a 45 mm diameter area exposed to the solution at the bottom side of the plate, i.e., on the side away from the SQUID magnetometer.

The X-Y scanning of the corrosion cell was computer controlled. The scanning area was larger than the sample for all tests. The scanning rate in x-direction was 20 mm/s, and the orthogonal step in y-direction after each scan was 1 mm or 3 mm. The data acquisition rate was 4 points per mm in the x-direction. The magnetic field distribution for the sample was measured as a function of time by the SQUID magnetometer. For each test, the magnetic field distribution for the sample in air, without the corrosive environment, was also measured before and after the sample was exposed to the solution.

3. Experimental Results

3.1. Magnetic Field Measured by SQUID During Active Corrosion of Aluminum Alloys in the Test Described by Figure 1a

3.1.1. Magnetic Field Measured by SQUID on 7075 and 2024 Aluminum Alloys Undergoing Pitting and/or Intergranular Corrosion

Figure 2a-2c show typical magnetic field distributions detected by the SQUID near the surface of actively corroding 7075 aluminum alloy plate in a solution of 3.5% NaCl + 50 ppm Cu^{++}. The data shown in Figures 2a and 2b were obtained over periods of 25 to 43 minutes and 205 to 223 minutes after the sample was placed in the solution, respectively, which is considered to be representative of the interval involved in the initiation of pitting, and in Figure 2c over the period of 275 to 293 minutes, which are considered to be representative of the time involved in the growth of these pits. Figure 2d shows the magnetic field distribution over the

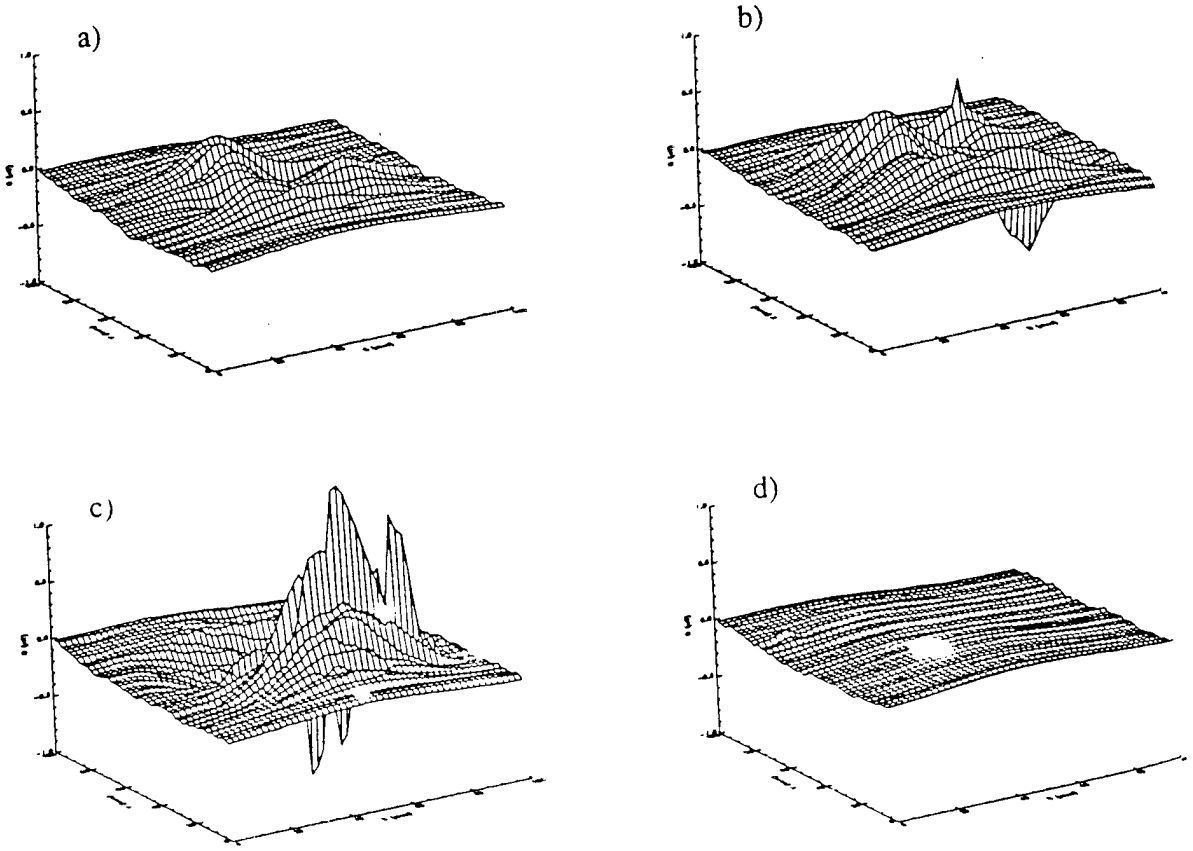

Figure 2. Typical magnetic field distributions for active pitting corrosion of a 32×32 mm 7075 aluminum alloy plate in a solution of 3.5% NaCl + 50ppm Cu^{++}. Data were obtained (a) in the time interval from 25 to 43 minutes after the sample was placed in the solution , (b) in the time interval from 205 to 223 minutes, (c) in the time interval from 275 to 293 minutes, and (d) in air after the corrosion attack.

sample in the absence of a corroding environment, after the corrosion attack. The above results give evidence that the magnetic fields measured by the SQUID magnetometer are due solely to corrosion current.

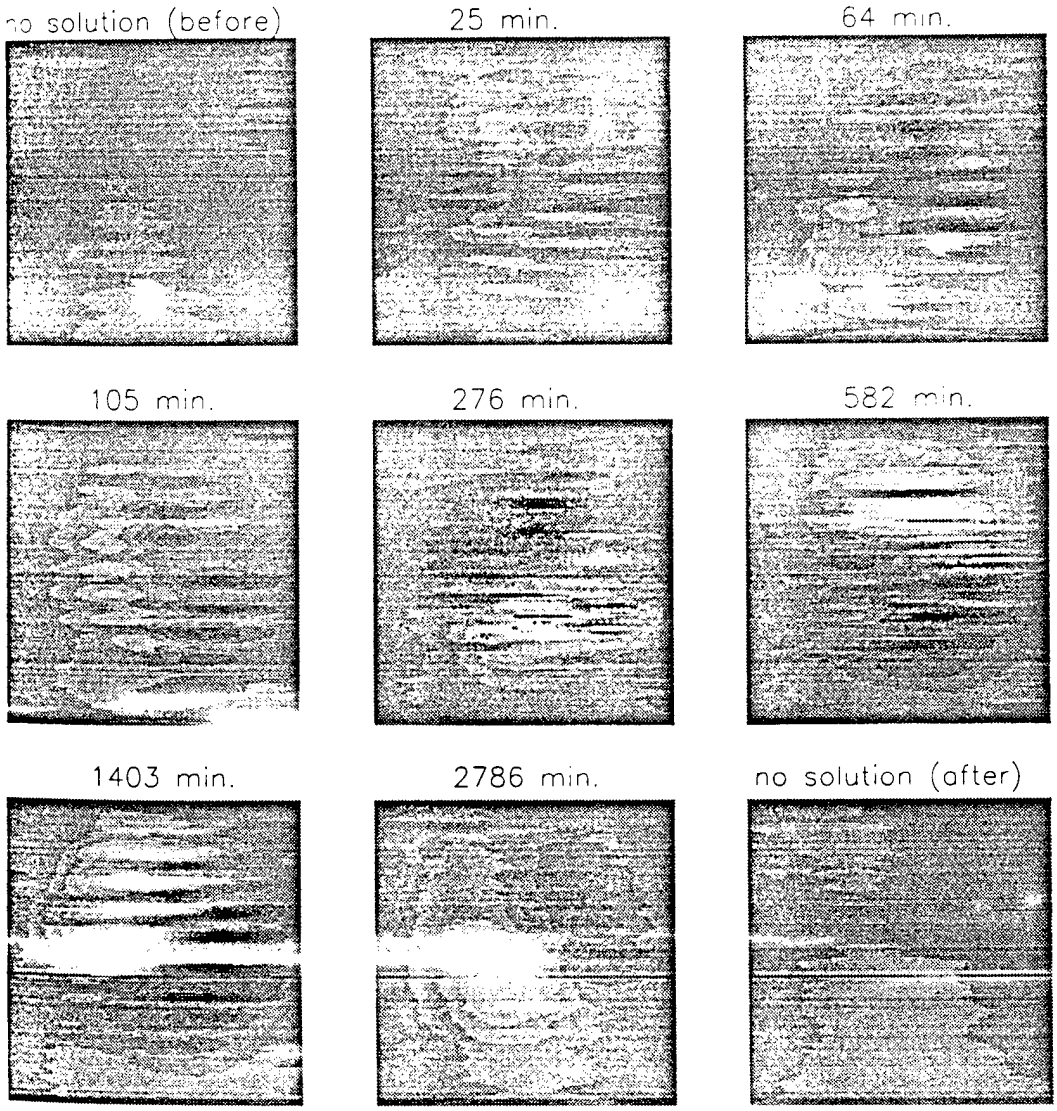

Figure 3. The magnetic field as a function of time during active pitting corrosion of a 32×32 mm 7075 aluminum alloy plate in a solution of 3.5% NaCl + 50 ppm Cu^{++}.

Figures 3 and 4 show typical magnetic field distributions on the sample as a function of time during active corrosion of 7075 and 2024 aluminum alloys, respectively, both in the same solution of 3.5% NaCl + 50 ppm Cu^{++}. Such

distributions are found to change from time to time, and are believed to be related to the variation of the local corrosion current in the sample.

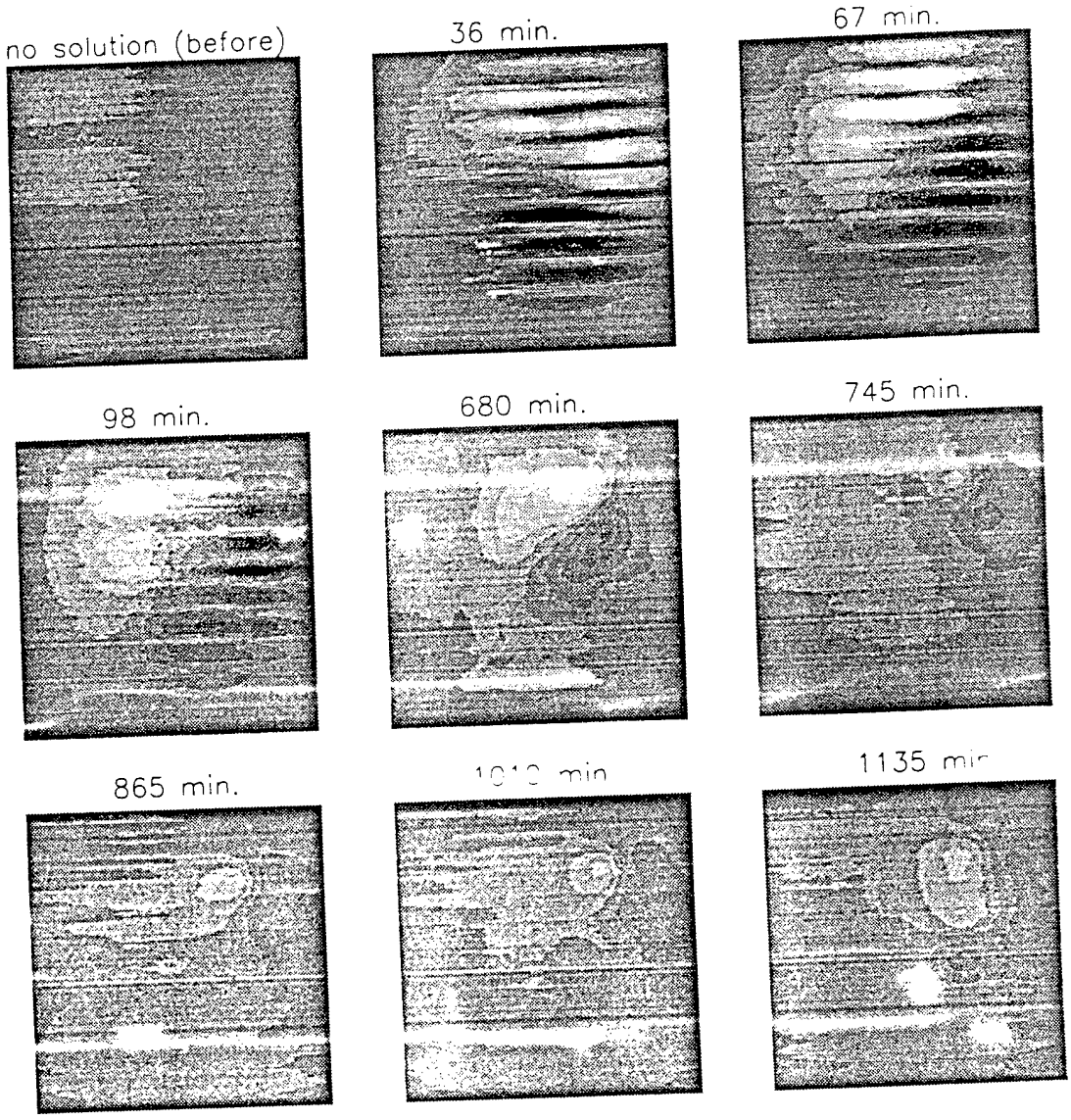

Figure 4. The magnetic field as a function of time during active corrosion of a 32×32 mm 2024 aluminum alloy plate in a solution of 3.5% NaCl + 50 ppm Cu^{++}.

Figure 5a and 5b show variation over time of the maximum positive and negative magnetic field density during active corrosion of 7075 and 2024 aluminum alloys in a solution of 3.5% + 50 ppm Cu^{++}, respectively. It is shown that this change is clearly different for the two alloys. Figures 6a and 6b show the variation of the maximum positive magnetic field density with Cu^{++} concentration for 7075

and 2024 aluminum alloy respectively during active corrosion at different times. It is seen that the difference of the maximum positive magnetic field density, as the Cu^{++} concentration varies from 10 ppm to 50 ppm, increases with time for 7075 aluminum alloy, but decreases with time for 2024 aluminum alloy. It is also shown that the maximum positive magnetic field density in the solution with 50 ppm Cu^{++} is larger than that in a solution with 10ppm Cu^{++}, for both the 7075 and 2024 aluminum alloys.

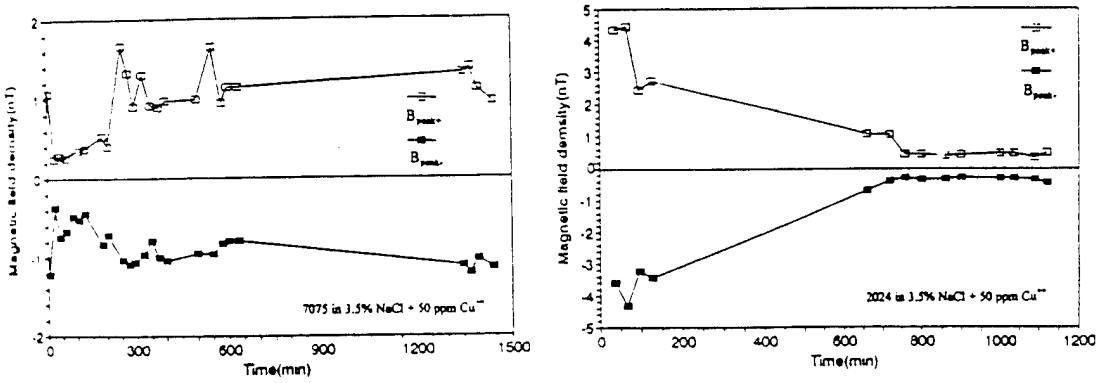

a) b)

Figure 5. The maximum positive and negative magnetic field density as a function of time during active corrosion of (a) 7075 and (b) 2024 aluminum alloys in a solution of 3.5% NaCl + 50 ppm Cu^{++}.

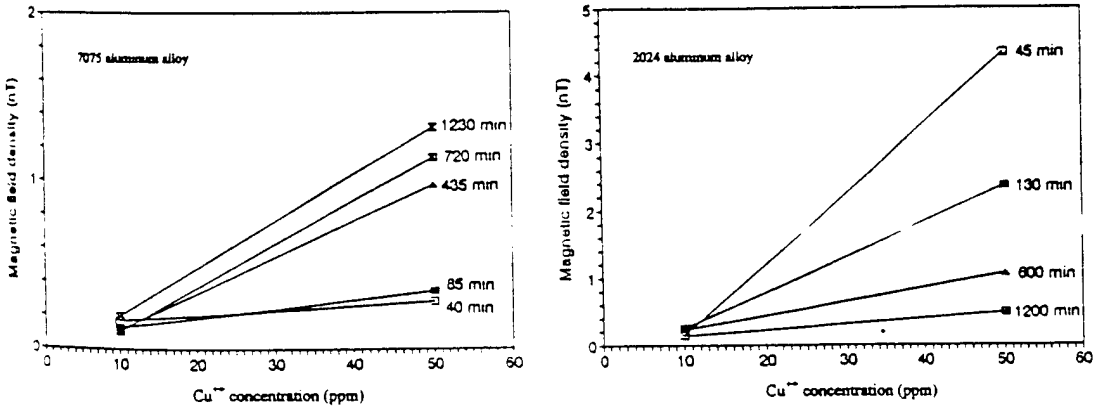

a) b)

Figure 6. Variation of maximum positive magnetic field density with Cu^{++} concentration at different times for active corrosion of (a) 7075 aluminum alloy and (b) 2024 aluminum alloy.

A typical microstructure for 7075 aluminum alloy after corrosion is shown in Figure 7a; this involved a cumulative exposure time of about 1440 minutes in 3.5% NaCl + 50 ppm Cu^{++}. Figure 7b shows the corresponding microstructure for 2024

aluminum alloy after a cumulative exposure of 1220 minutes in an identical solution. The attack in the 7075 aluminum alloy was found to penetrate as pits deep into the sample, while the attack in the 2024 aluminum alloy was found to be mainly surface attack at grain boundaries and localized pits.

a) 7075(160X)

b) 2024(160X)

Figure 7. Typical microstructures of 7075 and 2024 aluminum alloys after active corrosion in a solution of 3.5% NaCl + 50 ppm Cu^{++} in the SQUID tests.

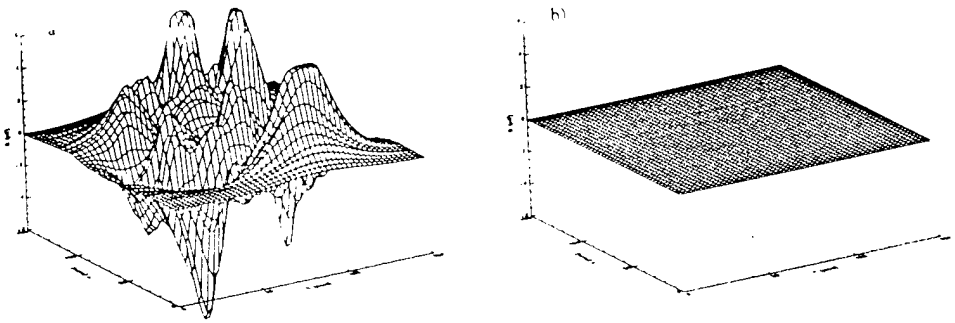

Figure 8. Typical magnetic field distributions for a 113 mm diameter circular plate of 2024 aluminum alloy undergoing active "uniform" corrosion in a solution of 2 ml 58% HF, 3 ml 71% HNO_3, 5 ml 36.5% HCl, and 590 ml H_2O. Data was obtained (a) over the period from 183 to 198 minutes after the sample was placed in the solution , and (b) in air after the corrosion attack .

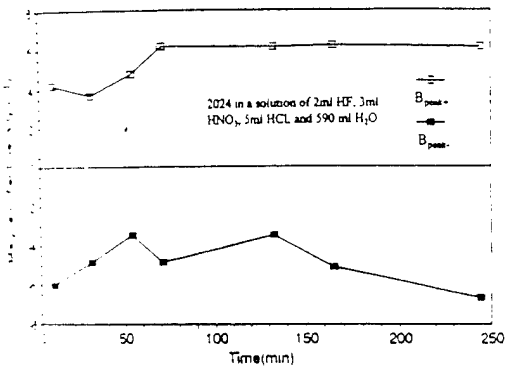

Figure 9 The maximum positive and negative magnetic field density as a function of time during active "uniform" corrosion of 2024 aluminum alloys in a solution of 2 ml 58% HF, 3 ml 71% HNO_3, 5 ml 36.5% HCl, and 590 ml H_2O.

160X

Figure 10. Typical microstructure of 2024 aluminum alloys after "uniform" corrosion in a solution of 2 ml 58% HF, 3 ml 71% HNO_3, 5 ml 36.5% HCl, and 590 ml H_2O.

3.1.2. Magnetic Field Measured by SQUID on 2024 Aluminum Alloy Undergoing "Uniform" Corrosion

Figure 8a shows a typical magnetic field distribution during "uniform" corrosion of 2024 aluminum alloy in a solution of 2 ml 58% HF, 3 ml 71% HNO_3, 5 ml 36.5% HCl, and 590 ml H_2O. Figure 8b shows the lack of any magnetic field distribution over the sample in the absence of the corroding environment after the corrosion attack. Figure 9 shows the variation of the maximum positive and negative magnetic field density with time during "uniform" corrosion. It is found that the change of the magnetic field density with time differs from that for pitting corrosion (Figures 5b and 9). The microstructure of 2024 aluminum alloy after "uniform" corrosion is shown in Figure 10, where it is seen that the attack is "uniform" over the sample surface.

3.2 Magnetic Field Measured by SQUID During Active Corrosion of Aluminum Alloys in the Test Described by Figure 1b

Figure 11a and 11b show typical magnetic field distribution detected by the SQUID for active corrosion of 2024 aluminum alloy plate, which has an 45 mm diameter area exposed to the solution at the bottom side of the plate, in solutions of 3.5% NaCl + 50 ppm Cu^{++} and 2 ml 58% HF, 3 ml 71% HNO_3, 5 ml 36.5% HCl, and 590 ml H_2O.

respectively. The results give evidence that the SQUID magnetometer is sensitive to corrosion activity occurring on the opposite side of a plate specimen.

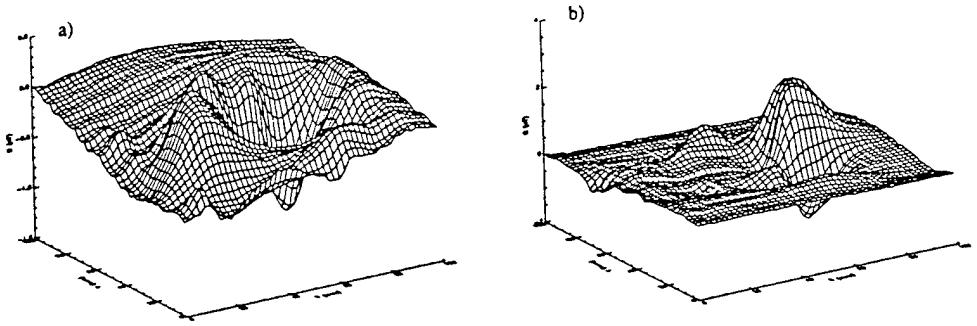

Figure 11. Typical magnetic field distribution measured by SQUID in the test described by Figure 1b for active corrosion of 2024 aluminum alloy (a) in a solution of 3.5% NaCl + 50 ppm Cu^{++} and (b) in a solution of 2 ml 58% HF, 3 ml 71% HNO_3, 5 ml 36.5% HCl, and 590 ml H_2O.

4. Discussion

4.1. Magnetic Field Distribution as an Indicator of the Type of Corrosion

It is seen from Figure 7 that the microstructure of 7075 aluminum alloy undergoing pitting corrosion differs from that of 2024 aluminum alloy which shows pitting/intergranular corrosion. It is also seen that the variation of the maximum positive and negative magnetic field density with time for the 7075 aluminum alloy in a solution of 3.5% NaCl + 50 ppm Cu^{++} (Figure 5a) is very different from the results for 2024 aluminum alloy in the identical solution (Figure 5b), and also that the variation of magnetic field density with time for 2024 aluminum alloy in the "uniform' corrosion solution is clearly different from that in the pitting solution (Figure 5b and Figure 9). These results give evidence that the SQUID can be used to distinguish between the different types of corrosion in 7075 and 2024 aluminum alloys.

4.2. Magnetic Field Intensity as an Indicator of Corrosion Rate

As we can see in Figures 6a and 6b, the magnetic field density in the solution of 3.5% NaCl containing 50 ppm Cu^{++} is larger than that in the solution containing 10 ppm Cu^{++}. This can be explained by the fact that when copper ions are added to a solution containing chloride ions, the corrosion potential of the aluminum alloy immediately rises close to the pitting potential[17,18]. The reason is that dissolved

Cu^{++} deposits on the aluminum alloy surface as metallic Cu, which acts as an efficient cathode, causing the corrosion potential of the aluminum alloy to shift up to near the pitting potential. The higher the Cu^{++} concentration in the solution, the more Cu^{++} is deposited on the aluminum alloy surface, and these cathodes in the aluminum alloy surface become more efficient. Figure 6a also shows that the increase of the extrema in the magnetic field density with time for 7075 aluminum alloy in the solution with 50 ppm Cu^{++} is much more rapid than that in the solution with 10 ppm Cu^{++}. This parallels the increase of corrosion current expected in each of these cases.

It is also seen that the maximum positive and negative magnetic field density for 2024 aluminum alloy in the "uniform" corrosion solution (Figure 9) is larger than that in the pitting solution (Figure 5b). This can be explained by the fact that the corrosion current of the sample in the former solution may be much larger than for that in the pitting case, i.e., the higher the corrosion current, the more intense is the magnetic field. The magnetic field density for 2024 aluminum alloy in the solution of 3.5% NaCl + 50 ppm Cu^{++} is larger than that for 7075 aluminum alloy in the identical solution for up to 700 minutes after the samples were placed in the solution (Figures 5a and 5b). This difference may be explained by the fact that different corrosion mechanisms are involved, so that different corrosion currents result. These facts also attest to the feasibility of using SQUID results to measure corrosion currents. The magnetic field distribution as affected by the geometry of the test sample and cell was also studied, and the results will be reported in a later paper.

5. Conclusions

1. Magnetic field distributions resulting from active in-situ corrosion in aluminum alloy samples can be measured by SQUID magnetometry.
2. The variation of maximum positive and negative magnetic field density with time is clearly different for the three types of active in-situ corrosion studied, allowing one to use SQUID magnetometry as an indicator of the type of corrosion that is actively involved.
3. The magnetic field density is an indicator of the magnitude of active in-situ corrosion occurring in the specimen.
4. The SQUID magnetometer is sensitive to corrosion activity occurring on the opposite side of a plate specimen.

Acknowledgments

This work is supported by Air Force of Scientific Research grant F49620-93-0268.

6. References

1. H.S. Isaacs, G. Kissel, J. Electrochem. Soc., 119, 1628(1972)
2. L.J. Gainer, G.R. Wallwork, Corrosion, 35,2,61(1979)
3. H.S. Isaacs, M.W. Kendig, Corrosion, 36, 6, 269(1980)
4. R.J. O'Halloran, L.G. Williams, and C.P. Lloyd, Corrosion, 40,7,344(1984)
5. H.S. Isaacs, Corrosion, 43,10,594(1987)
6. J.G.Bellingham, M.L.A. MacVicar, M. Nisenoff, P. Searson, J. Electrochem. Soc., 133, 8, 1753(1986)
7. J.G. Bellingham, M.L.A. MacVicar, M. Nisenoff, IEEE Trans. MAG., MAG-23, No.2, 477(1987)
8. Mira Misra, Scott Lordi, and M.L.A. MacVicar, IEEE Trans. MAG., 27, 2, 3245(1991)
9. J.C. Murphy, G. Hartong, R.F. Cohn, P.J. Moran, K. Bundy, and J.R. Scully, J. Electrochem. Soc., 135, 2, 310(1988)
10. J.C. Murphy, R. Srinivasan, and R.S. Lillard, Rev. of Progress in QNDE, D.O. Thompson and D.E. Chimenti, Eds., Plenum, NY, Vol. 8B, pp. 2149(1989).
11. D.S. Buchanan, D.B. Crum, D. Cox, and J.P. Wikswo, Jr., Adv. in Biamagnetism, S.J. Williamson, G. Hoke, G. Stroink, and M. Kotani, Eds., pp. 667-679, Plenum, NY (1990).
12. Y.P. Ma and J.P. Wikswo, Jr., Rev. Sci. Instrum., Vol. 62, pp. 2654(1991).
13. J.P. Wikswo, Jr., J.M. van Egeraat, Y.P. Ma, N.G. Sepulveda, D.J. Staton, S. Tan, and R.S. Wijesinghe, Digital Image Synthesis and Inverse Optics, A.F. Gmitro, P.S. Idell, and I.J. LaHaie, Eds., Vol. 1351, pp. 438-470, SPIE Proceedings(1990).
14. Y.P. Ma, D. J. Station, N.G. Sepulveda, and J.P. Wikswo, Jr., Rev. of Progress in Quantitative Nondestructive Evaluation, D.O. Thompson and D.E. Chimenti, Eds., Vol. 10A, pp. 979-986, Plenum, NY(1991).
15. J.P. Wikswo, Jr., D.B. Crum, W.P. Henry, Y.P. Ma, N.G. Sepulveda, and D.J. Station, J. of Nondestructive Evaluation, 12, 2, 109(1993).
16. Y.P. Ma and J.P. Wikswo,Jr., Rev. of Progress in Quantitative Evaluation, D.O. Thompson and D.F.Chimenti, Eds., Vol. 11A, pp.1153-1159, Plenum. NY(1992).
17. H.H. Uhlig, J. Electrochem. Soc., 116, 906(1969).
18. S. Furuya and S. Soga, Corrosion, 46, 989(1990).